JOC The Journal of Organic Chemistry

Article

pubs.acs.org/joc

Inclusion Compound Based Approach to Arrays of Artificial Dipolar Molecular Rotors: Bulk Inclusions

Lukáš Kobr,[†] Ke Zhao,[‡] Yongqiang Shen,[‡] Kateřina Polívková,[§] Richard K. Shoemaker,[†] Noel A. Clark,[‡] John C. Price,[‡] Charles T. Rogers,[‡] and Josef Michl*[,†,§]

[†]Department of Chemistry and Biochemistry and [‡]Department of Physics, University of Colorado, Boulder, Colorado 80309, United States

[§]Institute of Organic Chemistry and Biochemistry, Academy of Sciences of the Czech Republic, 16610 Prague 6, Czech Republic

Supporting Information

ABSTRACT: We examine the insertion of two dipolar molecular rotors as guests into a host, tris(*o*-phenylenedioxy)cyclotriphosphazine (TPP, **1**), using differential scanning calorimetry, solid-state NMR, powder X-ray diffraction, and dielectric spectroscopy. The rotors are 1-(4′-*n*-pentylbiphenyl-4-yl)-12-(2,3-dichlorophenyl)-*p*-dicarba-*closo*-dodecaborane and 1,12-bis-(2,3-dichlorophenyl)-*p*-dicarba-*closo*-dodecaborane. Both enter the bulk even though their nominal diameter exceeds the nominal channel diameter and although a closely related rotor, 1-*n*-hexadecyl-12-(2,3-dichlorophenyl)-*p*-dicarba-*closo*-dodecaborane, is known to produce a surface inclusion compound. Rotational barriers of 5.4−9.3 kcal/mol were found for the dichlorophenyl rotator contained within the TPP channel. Clearly, van der Waals diameters in themselves do not suffice to predict TPP channel entry. It is suggested that the efficacy of the *p*-carborane stopper is reduced by the presence of the two relatively bulky adjacent benzene rings, which help to stretch the channel, and by the axial direction of its axis, which prevents the attached rotator from contributing to the stopping action.

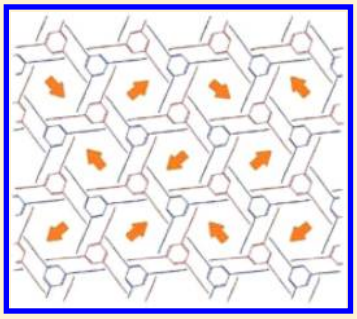

INTRODUCTION

Molecular rotors have received much attention,[1−7] and purposely designed regular arrays of interacting dipolar rotors would be expected to show interesting collective properties. They might also be of practical utility, e.g., as ultrafast dielectric materials in electronics, especially if they had a ferroelectric ground state. Rotor arrays with designed properties such as inter-rotor interactions are not easy to produce by growing crystals of neat molecular rotor compounds,[8−12] since many features need to be controlled simultaneously: the highly polar rotors must have very low rotational barriers, and the orientation of their axes as well as their geometrical arrangement and spacing need to be optimized. The issue has been recently discussed,[13] and it was proposed that the desired arrays might be produced by inserting the rotors as guests into channels in suitable hosts, allowing a separate tuning of the properties of the guest and the host. A related idea is to use metallo-organic frameworks (MOFs).[14,15] If the guests in a guest−host inclusion compound were constrained to the surface of the host, a two-dimensional (2-D) rotor array would result, and if they penetrated into the bulk, a three-dimensional (3-D) array would be produced. In a 3-D array, proper registry of rotors located in different channels might be difficult to achieve, but the total density of rotors in a thin layer of material would be much larger and the dielectric response stronger. However, even in a 2-D array the response would still be readily detectable.[3]

We have chosen as host hexagonal tris(*o*-phenylenedioxy)-cyclotriphosphazene **1** (TPP), whose crystals are composed of ∼5 Å thick layers penetrated in the perpendicular direction by a trigonal array of parallel hollow channels of 4.5−5 Å diameter, separated by ∼11.5 Å.[16] Their internal shape is locally triangular, with the triangles rotated by 60° from layer to layer (Figure 1). They readily include small molecules as guests,

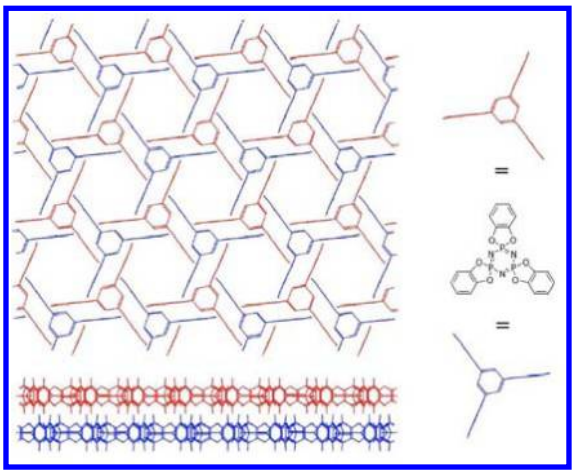

Figure 1. Crystal structure of hexagonal TPP.[16] Above, top view, and below, side view of two layers of the solid.

Special Issue: Howard Zimmerman Memorial Issue

Received: June 15, 2012

dx.doi.org/10.1021/jo3009897 | J. Org. Chem. XXXX, XXX, XXX−XXX

as shown by X-ray diffraction and solid-state NMR spectroscopy.[16−22] The inclusion of guests is easy to detect, since the solid-state NMR chemical shifts of their nuclei are displaced by several ppm by the ring currents in the TPP host. An even easier way is to use TPP-d_{12} as host and look for cross-polarization of TPP carbons by magnetized protons of the guest.[13] TPP also forms monoclinic crystal modification that does not form inclusion compounds and whose presence is readily recognized in NMR spectra and X-ray diffraction patterns.[17,23,24] Below about 150 °C, the monoclinic form is the more stable crystal modification in the absence of a guest.

Having chosen hexagonal TPP as the host, we need to design the molecular rotor guest to produce regular arrays. First, we need to ensure the formation of an inclusion compound, which reflects a competition between the cohesive forces in the crystal of a neat dipolar rotor guest and the attractive forces between the guest and the TPP channel walls. A tight fit of the rotor into the TPP channel is desirable to maximize this attraction and also to anchor the rotator axle firmly along the channel axis, but excessively thick guests may encounter steric hindrance to inclusion and fail to enter. TPP channels are able to expand to some degree in response to the presence of a guest,[25] but little is known presently about the maximum lateral dimensions of an acceptable guest.[26]

Three insertion modes are of interest (Figure 2): (mode A) surface inclusion, with the dipolar rotating part (rotator) located outside the host; (mode B) surface inclusion, with the dipolar rotator inside the host; and (mode C) bulk inclusion, with the whole molecular rotor including the rotator inside the host.

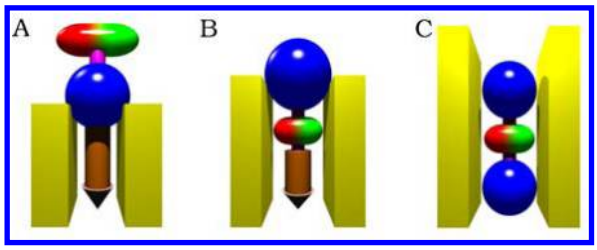

Figure 2. Three modes of guest inclusion. (A) Surface inclusion, with the dipolar rotating part (rotator) located outside the host; (B) surface inclusion, with the dipolar rotator inside the host; and (C) bulk inclusion, with the whole molecular rotor including the rotator inside the host.

In a triangular lattice, good registry of the dipolar rotators in a surface inclusion will be most likely opposed by their electrostatic interactions and will require the guest molecules to have high affinity for the channel walls. For a 2-D surface inclusion, we therefore attach the dipolar rotator to a relatively long shaft, and we prevent the entry of the whole rotator molecule inside the channel by terminating the shaft with a sufficiently bulky stopper. For insertion mode A, we search for suitable guests of the type shaft−stopper−rotator and for mode B, for guests of the type shaft−rotator−stopper. Mode A has the advantage that electrostatic inter-rotator interactions are not attenuated by the dielectric constant of the host. For mode C, guests of the type shaft−rotator, shaft−rotator−shaft (shown in Figure 2), or even rotator−shaft−rotator would all appear possible, with the diameter of the shaft in excess of that of the rotator. In this instance, the shafts would not only fix the direction of the rotational axis, but also help control the distance between dipolar rotators within the same channel in order to reduce the intrachannel electrostatic coupling, which should not exceed interchannel coupling if the ground state is to be ferroelectric.

In our first publication on the subject,[13] we reported the formation of a surface inclusion compound of type A from a shaft−stopper−rotator guest but found that in samples with high channel occupancy, the guests were not all inserted to the same depth, suggesting imperfect registry of the rotators at the surface. Barriers to rotation were relatively high (1.2−9 kcal/mol), presumably because of a deviation of the rotator axle from the surface normal and a resulting close contact of the rotator with the surface at certain rotation angles. Presently, we report results for an inclusion of type C, with 1-(4′-*n*-pentylbiphenyl-4-yl)-12-(2,3-dichlorophenyl)-*p*-dicarba-*closo*-dodecaborane (**2**) and 1,12-bis(2,3-dichlorophenyl)-*p*-dicarba-*closo*-dodecaborane (**3**), shown in Chart 1, as guests in TPP. Results for a different inclusion type C are being reported elsewhere.[26]

Chart 1. Molecular Structures of the Host (1) and Guests (2, 3)

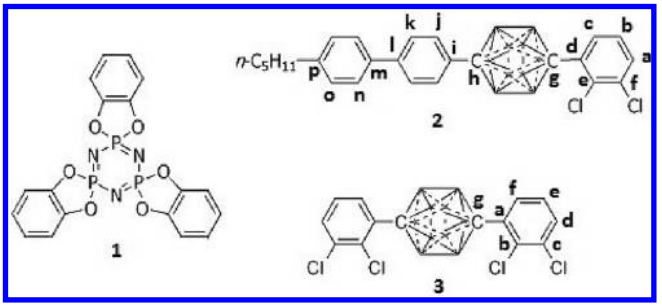

RESULTS

The ease with which benzene enters TPP channels to form benzene@TPP[16] suggested that biphenyl will form an inclusion compound biphenyl@TPP as well, and indeed it does (Supporting Information, Figure S1). This result suggested that oligophenyls might make good rotor shafts. Unlike the long alkyl chain used in our first paper,[13] they are expected to direct the rotator axle perpendicular to the surface as desired. In the following, we report the synthesis of **2** and **3**, assignment of their liquid NMR spectra, formation of inclusion compounds with microcrystalline TPP and their characterization by differential scanning calorimetry (DSC), solid-state NMR spectra, X-ray powder diffraction, and dielectric spectroscopy.

Synthesis. To make rotor **2** (Scheme 1), an organozinc reagent was prepared from *p*-(*n*-pentyl)bromobenzene and Negishi coupled with *p*-iodonitrobenzene to **4** in 84% yield. The product was reduced to **5** in 94% yield and converted to **6** 84% yield by the Sandmayer reaction.

Ulmann coupling with the cuprous salt of *p*-carborane to yield **7**, analogous to previous work,[27] proceeded in 92% yield. A small amount of the disubstituted product was also formed. When the reaction was tried under catalysis with various palladium(0) catalysts, much *p*-(*n*-pentyl)biphenyl was formed, and the yield of **7** was low. Addition of triethylamine to the reaction mixture increased the yield, but the Ulmann conditions remained superior. Ulmann-type reaction of **7** with 1,2-dichloro-3-iodobenzene provided **2** in 87% yield. This procedure was again better than using palladium as catalysts.

dx.doi.org/10.1021/jo3009897 | J. Org. Chem. XXXX, XXX, XXX−XXX

Scheme 1. Synthesis of 2

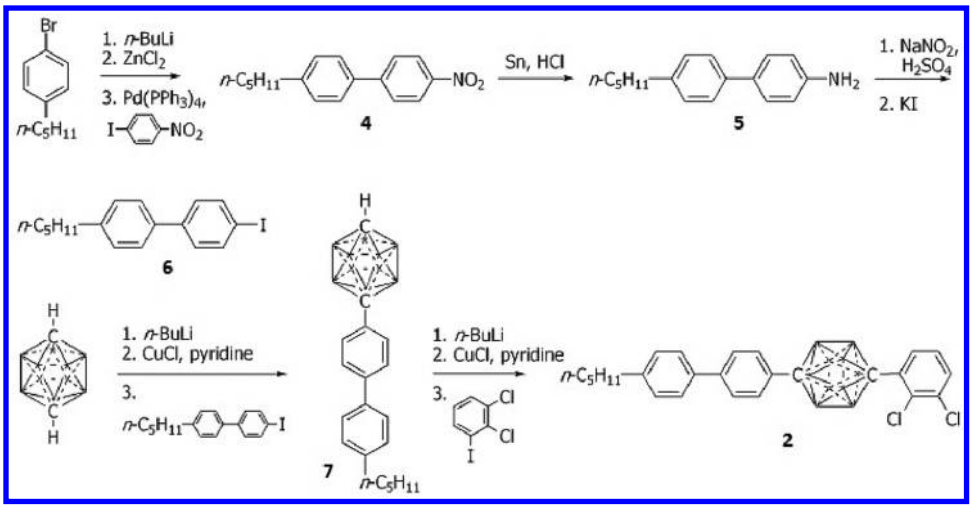

The rotor **3** was prepared by Ulmann coupling in 76% yield (Scheme 2), and the preparation of TPP-d_{12} (isotopic purity >99.8%) has been described.[13]

Scheme 2. Synthesis of 3

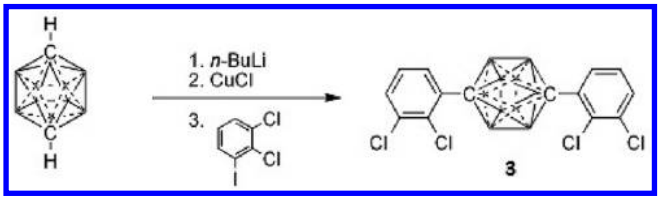

Solution NMR (Chart 1 and Figure 3). The assignment of carbons and protons in **2** (Table 1) was deduced from their ^{1}H NMR, ^{13}C NMR, ^{1}H–^{1}H gCOSY (Supporting Information, Figure S2, top), ^{1}H–^{13}C gHSQC (Supporting Information, Figure S2, bottom), ^{1}H–^{13}C gHMBC, (Figure S3, top), and boron decoupled ^{1}H–^{13}C gHMBC (Supporting Information, Figure S3, bottom) spectra as described in the Supporting Information.

A detailed assignment of the spectrum of **3** was not needed. Of the six resolved aromatic signals in its ^{13}C NMR spectrum, C_a, C_b and C_c belong to the quaternary carbons of the 2,3-dichlorophenyl rotators, and C_d, C_e and C_f to the protonated carbons, on the basis of DEPT135. The signal C_g belongs to the *p*-carborane carbons.

Formation and DSC of Inclusion Compounds 2@TPP and 3@TPP. Two procedures for the formation of inclusion compounds from solids were tested. Grinding yielded the TPP inclusion of 5 mol % of **2** (5%**2**@TPP). Ball milling followed by annealing was used to obtain 15%**2**@TPP-d_{12} and 15%**3**@TPP-d_{12}.

The DSC results are shown in the Supporting Information (Figures S4 and S5). The trace of hexagonal TPP-d_{12} consists of a broad exotherm centered around 148 °C and endotherms at 222 and 252 °C.[13] The neat **2** yields a single endotherm at 152 °C, and 15%**2**@TPP-d_{12} yields two very broad exotherms at 100 and 210 °C and two endotherms at 251 and 282 °C. Neat **3** gives a single endotherm at 265 °C, and 15%**3**@TPP-d_{12}, three endotherms at 232, 240, and 246 °C.

Solid-State NMR. The solid-state ^{13}C CP MAS NMR spectrum of neat **2** (Figure 3) shows chemical shifts and a pattern that are similar to the ^{13}C solution spectrum, except that some signals are split into two peaks, suggesting that two inequivalent crystallographic orientations are present in the unit cell.

The solid-state ^{13}C CP MAS NMR spectrum of 5%**2**@TPP (Figure 3) displays three large resonances in the aromatic region that are due to TPP. It also shows a pattern for the resolved guest peaks that is similar to the solution ^{13}C spectrum of **2**, but most are shifted upfield with respect to both the solution and the solid ^{13}C NMR spectra. Annealing sharpened the signals. The carbons of TPP now exhibit multiple signals since the empty portion of TPP became monoclinic.

Table 1. Summary of the ^{1}H and ^{13}C Assignments in Rotors 2 and 3 (cf. Chart 1)

2									3		
atom	^{1}H δ/ppm	^{13}C δ/ppm	atom	^{1}H δ/ppm	^{13}C δ/ppm	atom	^{1}H δ/ppm	^{13}C δ/ppm	atom	^{1}H δ/ppm	^{13}C δ/ppm
a	7.41*	131.02	h		86.60	o	7.24	129.02	a–c		131.40
											134.02
b	7.08	126.66	i		134.96	p		142.75			
											135.95
c	7.59	130.69	j	7.30	127.49	q	2.64	35.73			
d		134.19	k	7.41*	126.73	r	1.65	31.70	d–f	7.41	126.71
e		131.46	l		141.55	s	1.36*	31.29		7.07	130.53
										7.56	131.15
f		135.90	m		137.32	t	1.36*	22.71			
g		81.70	n	7.44	126.98	u	0.91	14.20	g		77.36

dx.doi.org/10.1021/jo3009897 | J. Org. Chem. XXXX, XXX, XXX–XXX

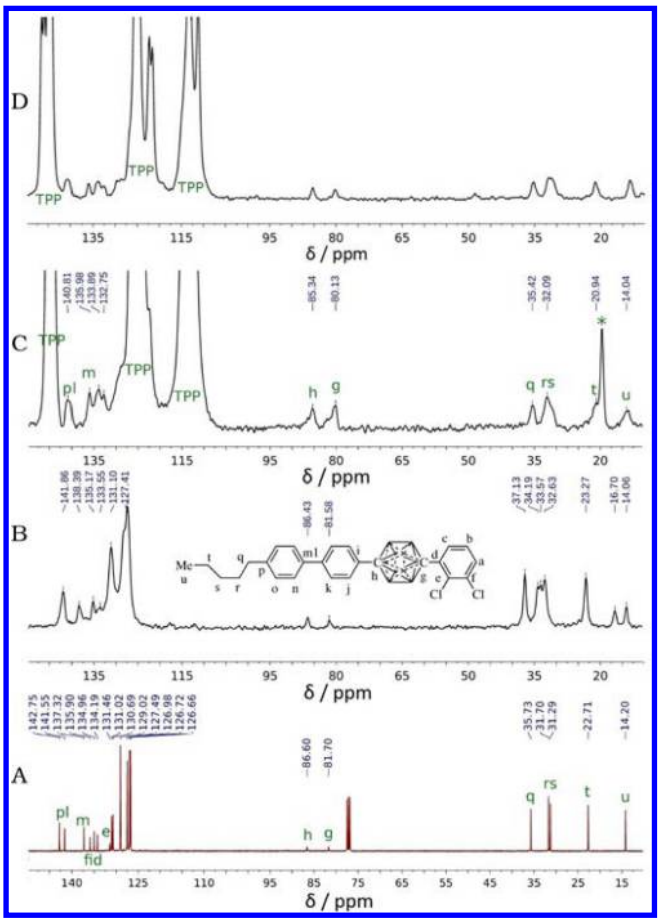

Figure 3. Solid-state ^{13}C CP MAS (5 ms contact time) and solution ^{13}C NMR spectra of **2**. (A) Solution of **2** in $CDCl_3$; (B) neat solid **2**; (C) solid 5%**2**@TPP; (D) annealed solid 5%**2**@TPP. *: a spinning sideband.

The solid-state ^{31}P SPE MAS NMR spectrum of 15%**2**@TPP-d_{12} (Figure 4) shows a singlet at 34.1 ppm, due to TPP-d_{12} in hexagonal form, and a few small signals around 0 ppm. The solid-state ^{13}C CP MAS NMR spectra of 15%**2**@TPP-d_{12} are shown in Figure 4.

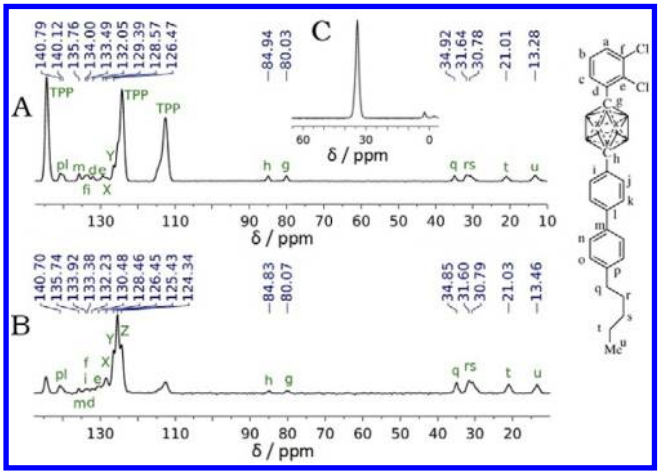

Figure 4. NMR spectra. (A) ^{13}C CP MAS (5 ms) of 15%**2**@TPP-d_{12}; (B) ^{13}C CP MAS (0.2 ms) of 15%**2**@TPP-d_{12}; (C) ^{31}P SPE MAS NMR of 15%**2**@TPP-d_{12}.

The long contact time spectrum shows three intense singlet aromatic resonances that belong to TPP-d_{12}. These three signals and the differences from the spectrum of neat **2** provide additional evidence for the formation of the inclusion compound. In the short contact time spectrum the signals of protonated carbons are enhanced relative to those of quaternary carbons. A comparison of the two spectra shows that the signals C_p, C_l, C_m, C_f, C_i, C_d, C_e, C_h, and C_g belong to quaternary carbons, while the signals X, Y, Z, C_q, C_r, C_s, C_t, and C_u belong to protonated carbons. The signals C_p, C_l, C_m, C_f, C_i, C_d, C_e, C_h, C_q, C_r, C_s, C_t and C_u, in the solid-state ^{13}C NMR spectrum of 15%**2**@TPP-d_{12} were tentatively assigned by comparison with the solution ^{13}C NMR spectrum of **2**. The chemical shifts in the solid-state ^{13}C NMR spectrum of 15%**2**@TPP-d_{12} are displaced upfield from their positions in the solution ^{13}C spectrum of **2**. The chemical shift changes for the resolved carbons are summarized in Table 2. The protonated aromatic carbons are not fully resolved, but they all display an upfield change in the chemical shift.

Table 2. Differences in the Chemical Shifts of 15%2@TPP-d_{12} and of the Solution Spectrum of 2

carbon	Δδ ppm	carbon	Δδ ppm	carbon	Δδ ppm	carbon	Δδ ppm
d	−2.1	h	−1.7	p	−2.0	t	−0.7
e	−1.1	i	−1.5	q	−1.8	u	−0.9
f	−1.9	l	−1.4	r	−0.1		
g	−1.7	m	−1.7	s	−0.5		

The solid-state ^{13}C CP MAS NMR spectra of neat **3** and 15%**3**@TPP-d_{12} are shown in Figure 5.

The solid-state ^{13}C CP MAS NMR spectrum of 15%**3**@TPP with dipolar dephasing only shows signals of nonprotonated carbons, while that of **3** with a short (0.2 ms) contact time displays protonated carbon signals enhanced relative to nonprotonated ones (Figure 5). A comparison of the two

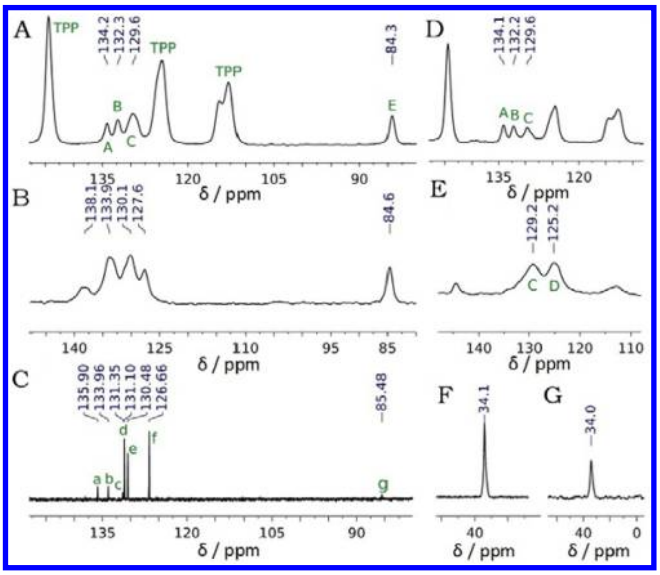

Figure 5. NMR spectra. (A) ^{13}C CP MAS of 15%**3**@TPP-d_{12}; (B) ^{13}C CP MAS of neat **3**; (C) ^{13}C of $CDCl_3$ solution of **3**; (D) ^{13}C CP MAS with DPD of 15%**3**@TPP-d_{12}; (E) ^{13}C CP MAS of 15%**3**@TPP-d_{12} with 0.2 ms contact time; (F) ^{31}P SPE MAS of 15%**3**@TPP-d_{12}; (G) ^{31}P CP MAS of 15%**3**@TPP-d_{12}.

dx.doi.org/10.1021/jo3009897 | J. Org. Chem. XXXX, XXX, XXX−XXX

spectra reveals that the signals A and B belong to quaternary aromatic carbons, and signal C contains protonated and nonprotonated carbon signals. The short contact time experiment shows an additional protonated carbon, D. A comparison of the solid-state ^{13}C NMR spectrum and the solution spectrum of **3** suggests that carbon C_a gives rise to the signal A in the inclusion compound solid-state spectrum, carbon C_b is responsible for signal B, and a part of the signal C belongs to carbon C_c. The remaining intensity of signal C and signal D belong to the protonated carbons C_d, C_e and C_f. Signal E belongs to the *p*-carborane carbons C_g. The solid-state ^{31}P SPE MAS NMR and ^{31}P CP MAS NMR both show a single resonance at 34.1 and 34.0 ppm, respectively (Figure 5). All the aromatic signals of **3** in 15%**3**@TPP-d_{12} are shifted upfield relative to the solution ^{13}C NMR spectrum of **3**, and the *p*-carborane carbons are shifted upfield by 1.2 ppm.

X-ray Powder Diffraction. The same solid-state NMR samples 15%**2**@TPP-d_{12} and 15%**3**@TPP-d_{12} were also used for copper $K_{\alpha 1}$ wavelength X-ray powder diffraction measurements. Figure 6 shows the scattered X-ray photon counts versus the magnitude of the scattering wave vector q, related to scattering angle θ and X-ray wavelength λ by $q = 4\pi \sin\theta/\lambda$.

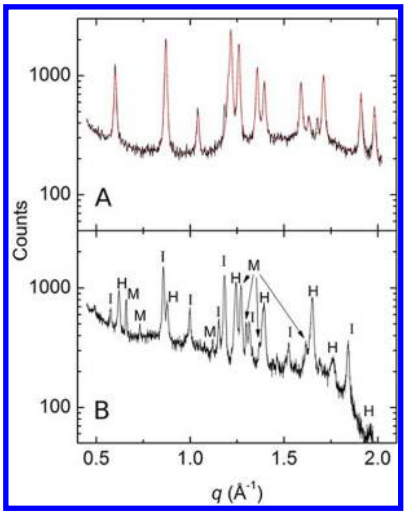

Figure 6. X-ray powder patterns from inclusion compounds. (A) 15%**2**@TPP-d_{12} (solid black line, diffraction data; red line, fit assuming hexagonal peak positions). (B) 15%**3**@TPP-d_{12} with assignments (H, empty hexagonal TPP; M, monoclinic TPP; I, a hexagonal inclusion compound).

The trace for 15%**2**@TPP-d_{12} shows a sequence of diffraction peaks that fit a single hexagonal structure with lattice parameters expanded in the in-plane direction to 12.067 ± 0.001 Å and contracted in layer spacing to 9.979 ± 0.001 Å. These values represent a 5.4% expansion and a 1.8% contraction, respectively, compared to the 11.454 ± 0.005 Å and 10.160 ± 0.005 Å values reported for empty hexagonal TPP.[28] Peak widths suggest a typical powder particle size of 40 nm. These results demonstrate that 15%**2**@TPP-d_{12} adopts a global hexagonal structure, consistent with the local hexagonal structure shown by the solid state NMR data.

The trace for 15%**3**@TPP-d_{12} displays a complicated peak structure that is consistent with a mixture of empty TPP, monoclinic TPP, and a single hexagonal structure with in-plane lattice parameter of 12.56 ± 0.01 Å and a layer spacing of 10.10 ± 0.01 Å. These values are expanded by by 9.7% and contracted by 0.6%, respectively, relative to empty TPP. From peak widths, the particle size for the hexagonal 15%**3**@TPP-d_{12} present in the mixture is 100 ± 20 nm.

Dielectric Spectroscopy. The results of dielectric loss measurements on the same samples of 15%**2**@TPP-d_{12} and 15%**3**@TPP-d_{12} that were used for NMR and X-ray diffraction studies are shown in Figure 7. 15%**2**@TPP-d_{12} displays

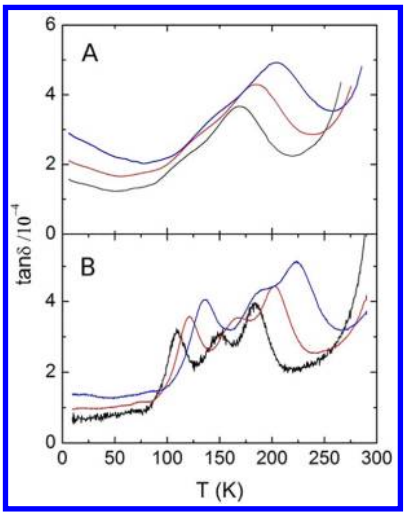

Figure 7. Dielectric loss at 120 Hz (black), 1200 Hz (red), and 12 kHz (blue). (A) 15%**2**@TPP-d_{12}; (B) 15%**3**@TPP-d_{12}.

primarily a single barrier to rotation, with a slight shoulder on the low temperature side. The barrier has a height E_b of 8.90 ± 0.02 kcal/mol, the frequency factor A is (2.2 ± 0.2) × 10^{13} Hz, and the asymmetry parameter s is 0.52 ± 0.01 kcal/mol. The shoulder can be fitted to E_b = 4.70 ± 0.03 kcal/mol, A = (5.1 ± 0.6) × 10^{12} Hz, and s = 0.92 ± 0.02 kcal/mol. 15%**3**@TPP-d_{12} has a more complicated set of three loss peaks. Listing from the lowest temperature peak to the highest, their E_b values are 5.37 ± 0.01, 6.73 ± 0.03, and 9.25 ± 0.04 kcal/mol, their A values are (1.5 ± 0.1) × 10^{13}, (2.0 ± 0.2) × 10^{13}, and (2.5 ± 0.3) × 10^{14} Hz, and their s values are 0.34 ± 0.01, 0.51 ± 0.01, and 0.68 ± 0.01 kcal/mol, respectively.

DISCUSSION

Choice of Guest. The rationale for choosing TPP as the host system has been described elsewhere,[13] and here we only need to note that (i) the nominal internal diameter of the channels available for the guest species is about 4.5−5 Å, that (ii) TPP is capable of expanding its lattice to accommodate even guests with a larger diameter, and that (iii) *p*-carborane (~7.6 Å across[29]) refused to enter TPP when it was attached to a long alkyl chain and carried a rotator in the antipodal position.

Guest rotors that form a 2-D surface inclusion compound, with a transverse dipole carrying rotator at the surface, either just outside (Figure 2A) or just inside (Figure 2B), would be particularly novel and attractive. Our first attempt to attain this goal with a rotor molecule consisting of a hexadecyl shaft, a *p*-carborane stopper, and a 2,3-dichlorophenyl rotator with a ~2.5 D dipole moment[30] was successful,[13] but the 2-D rotor array suffered from two shortcomings. First, the most concentrated samples, in which the TPP channels were close to saturated with the rotor guests, were heterogeneous. In these samples, different rotors were apparently inserted to different depths and

dx.doi.org/10.1021/jo3009897 | J. Org. Chem. XXXX, XXX, XXX−XXX

had different rotational barriers. Second, most of the barriers to rotation were too high to be useful, 1.2−9 kcal/mol, although in the model for the isolated molecule a barrier of only 1.56 kcal/mol was calculated.[13] The higher values were tentatively attributed to rotators that rubbed the surface because they were close to it and their axles did not lie along the surface normal.

Presently, we tried to solve the second difficulty by assuring that the rotator axle, whose direction is fixed by the C−C axis of the *p*-carborane stopper, lies perpendicular to the surface. Unlike the terminal bond of an alkyl chain, which does not lie along the long axis, that of a polyphenylene chain does, and for **2**, one can expect the C−C axis of the attached *p*-carborane to lie normal to the crystal surface. If the *p*-carborane stopper performed its intended function similarly as when it was attached to an alkyl chain, prevented entry of the rotator inside the guest channel, and forced it to remain just outside the TPP surface, an inclusion compound with a 2-D array of rotators with small barriers to rotation would result. The large (∼7.8 Å[31]) diameter of the *o*-dichlorobenzene rotator makes it unlikely that the rotor guest would enter the TPP channels rotator first; such orientation was not observed for the previously studied rotor molecule.[13] By analogy, we did not expect the double rotor **3** to form any inclusion compound with TPP. Below, we discuss the data obtained for **2**@TPP and **3**@TPP, both of which form bulk inclusions, illustrating how little it takes to thwart the best laid plans of mice and men.

Synthesis. The Ulmann conditions for the coupling of *p*-carborane to an iodo arene[27] produced good results in all the reactions necessary for the syntheses of **2** and **3**. In contrast, the more popular Pd-catalyzed coupling of halides with cuprous *p*-carborane derivatives was troublesome, most likely because of slow transmetalation of cuprous *p*-carborane derivatives with arylpalladium halides. The latter can apparently also undergo a competing reduction to *p*-(*n*-pentyl)biphenyl by the solvent or trace impurities in the solvent. This hypothesis is supported by the fact that when reducing solvents such as THF are avoided, the reduction is partially suppressed. The addition of ligands that are able to activate the copper in *p*-carborane for transmetalation, such as triethylamine, also suppresses the formation of *p*-*n*-pentylbiphenyl, but the classic Ulmann conditions remain superior.

Inclusion Compounds. The DSC traces in Figures S4 and S5 (Supporting Information) are compatible with the formation of inclusion compounds of TPP with both **2** and **3**. The nearly identical DSC traces of TPP[17,32] and TPP-d_{12}[13] are well understood. The single endotherm of neat **2** corresponds to melting. The two very broad exotherms in the DSC of 15%**2**@TPP-d_{12} are attributed to the first order transition of hexagonal TPP-d_{12} into its monoclinic form (100 °C) and further insertion of the guest rotors into TPP-d_{12} to form a hexagonal inclusion compound (210 °C). The endotherms are assigned to the melting of TPP-d_{12} (251 °C) and of the inclusion compound (282 °C). The origin of the small endotherm at 298 °C is unknown.

The first endotherm in the DSC trace of 15%**3**@TPP-d_{12} corresponds to the first order transition of monoclinic to hexagonal TPP-d_{12} and represents evidence for expulsion of the guest compound **3**. The two phase transitions at high temperatures are associated with the melting of TPP-d_{12} and of **3** at temperatures lower than the melting points of the pure components, due to the mixture effect.

NMR Spectra. The benzene ring was already known to enter TPP channels with ease,[16] and it was not a surprise when the differences in chemical shifts in the spectra of neat biphenyl and biphenyl@TPP (Figure S1, Supporting Information), and sharpening of the lines in the inclusion compound biphenyl@TPP, demonstrated that biphenyl enters as well. Biphenyl carbons of the inclusion compound exhibit both upfield and downfield changes in the chemical shifts relative to the ^{13}C NMR of neat solid biphenyl.

The detailed assignment of peaks in the solution ^{13}C NMR spectrum of **2** is unambiguous. In the spectrum of **3**, we have only distinguished the protonated from the unprotonated carbons of the benzene rings, and the carborane carbons. The solid-state ^{13}C NMR spectra of **2**@TPP and **3**@TPP show the same signal pattern as the solution spectra of the free guests. The differences in their chemical shifts relative to the solution spectra of **2** and **3** are much more consistent than the differences relative to the spectra of the neat solids **2** and **3**. The resolved aromatic signals in the ^{13}C solid-state spectra of the inclusion compounds were therefore assigned by comparison with the solution spectra. The differences in the chemical shifts are assumed to be due to the local magnetic anisotropy of the TPP environment, i.e., by its shielding and the deshielding effects. The assignments were verified by solid-state short-contact time and dipolar dephasing experiments.

Inclusion Compounds of Rotor 2 (Figures 3−5). The aromatic carbon assignments in the solid-state NMR spectrum of neat **2** cannot be reliably made by comparison with the solution spectrum, because the chemical shifts of the various aromatic carbons in the rotor **2** do not differ much. The solution spectra are averaged over all accessible conformations, while there is little conformational freedom in the solid. The effect of conformation on the chemical shift can be very strong and larger than the signal separation in the aromatic region of the ^{13}C NMR spectra of **2**.

5%2@TPP. Most signals in the solid-state ^{13}C CP MAS NMR spectrum of 5%**2**@TPP overlap with the middle TPP signal, and for interpretation it was necessary to reduce the TPP signal. This was achieved by using TPP-d_{12} instead of TPP. This also permits a quick detection of inclusion compound formation, since a mechanical mixture of a protonated compound with TPP-d_{12} containing no guests inside the channels will not give rise to any ^{13}C or ^{31}P NMR signal in the CP MAS experiment unless the contact times are very long. If the guest molecule is located within the channels, the ^{13}C or ^{31}P atoms of TPP-d_{12} become cross-polarized by the guest protons, demonstrating that an inclusion compound formed, and providing information on the local crystallographic structure of the host. By this criterion, **2** clearly makes an inclusion compound with TPP.

The annealing process greatly improves the homogeneity of the sample. The signals of TPP in the annealed sample split into several. Some belong to filled hexagonal TPP and the rest to empty TPP that collapsed into the monoclinic form during the annealing process.

15%2@TPP-d_{12}. The solid-state ^{31}P SPE MAS NMR (Figure 4) shows a singlet peak for the phosphorus atom of TPP-d_{12}, demonstrating that hexagonal TPP-d_{12} is present. The small signals around 0 ppm, a value of chemical shift typical for phosphates,[33] were assigned to impurities in TPP-d_{12} formed by oxidation during the annealing process.

The upfield changes in the ^{13}C chemical shifts of the shaft, the stopper and the rotator in the 15%**2**@TPP-d_{12} solid-state ^{13}C spectrum relative to the solution spectrum of **2** indicate that all the rotor parts are fully inserted inside the channel.

dx.doi.org/10.1021/jo3009897 | J. Org. Chem. XXXX, XXX, XXX−XXX

Some incompletely annealed samples were heterogeneous and contained more than one NMR peak for each carborane carbon, presumably due to the presence of a fraction of incompletely inserted guest molecules. The upfield changes in the chemical shifts of the aliphatic carbons in 15%**2**@TPP-d_{12} are smaller than those of remaining carbons. This is attributed to the presence of other chain conformations than anti in the solution and the averaging of their chemical shift into the observed value.[34] The aliphatic chains inside TPP are largely constrained to the anti conformation.[35,36]

The X-ray powder diffraction data indicate that the local structural information from solid-state NMR is also reflected in the longer range coherent structure. In the case of 15%**2**@TPP-d_{12}, the sample displays a single phase of hexagonal TPP structure in both the NMR and in the X-ray powder patterns. The expanded in-plane lattice parameter and slightly contracted layer spacing indicate how much the TPP channels have changed to allow for the insertion of a guest molecule. The nominal internal van der Waals diameter of TPP channels now is ∼5.15 instead of ∼4.95 Å, somewhat closer to the ∼6.7 Å value for the benzene ring, but still much smaller than the 7.8 Å values for *p*-carborane and 1,2-dichlorobenzene, which are both included nevertheless. This is apparently possible because of the "alternating triangle" nature of channels in TPP, which permits an inclusion of molecules with a larger than nominal diameter, as long as they fit into a single layer.

Using procedures described earlier,[3,13,14] dielectric spectroscopy yielded rotational barriers E_b, attempt frequencies A, and asymmetry parameters s. The results demonstrate that dipolar rotation in 15%**2**@TPP-d_{12} takes place with a single significant rotational barrier. This would be expected if all the rotors are in the same near-surface location, but it could be accounted for in other ways, too. Perhaps the TPP platelets are thin enough that all guest molecules are necessarily near the surface. The 15 mol % loading was selected as it is the rough molar percentage that one expects for a TPP platelet that is entirely populated on top and bottom by **2**, such that the rotator end is just barely immersed in the first TPP layer at the surface, and the ends of the alkane tails touch along the platelet midplane. This geometry offers the maximum surface to volume ratio for TPP crystallites, but additional investigations would be necessary to confirm that it is indeed present.

The considerable barrier height of 8.9 kcal/mol is consistent with the finding that the dipolar rotator is included within the host, whose channel is too narrow to accommodate it comfortably. The frequency factor is unexceptional and characteristic of molecular vibrational frequencies. The asymmetry factor of 0.5 kcal/mol is small compared to the barrier height and indicates that the rotator is moving in a largely symmetrical rotational potential as expected.

Inclusion Compounds of Rotor 3 (Figure 5). The solid-state ^{13}C NMR spectrum of 15%**3**@TPP-d_{12} is different from that of neat **3**. It shows three intense aromatic resonances that belong to TPP-d_{12} and signals A, B, C and D that belong to the guest compound **3**. The three TPP-d_{12} signals provide strong evidence for the formation of an inclusion compound. The splitting of the TPP-d_{12} signal located the farthest upfield into two peaks is attributed to TPP-d_{12} molecules of the filled channel and TPP-d_{12} molecules of unfilled or only partially filled channels. The latter are still in the proximity of the guest molecules **3**, since their carbons are cross-polarized.

The single resonance in the solid-state ^{31}P CP MAS NMR of 15%**3**@TPP-d_{12} is a result of cross-polarization between the guest protons and the phosphorus atoms of the TPP-d_{12} lattice. In absence of a guest with protons, TPP-d_{12} shows no ^{31}P signal. Therefore the single phosphorus signal in ^{31}P CP MAS NMR is an indication of inclusion compound of a hexagonal structure filled with guest molecules. The ^{31}P SPE MAS solid-state NMR reveals the structure of the entire sample, and the single peak in the spectrum of the inclusion compound shows hexagonal lattice throughout. The upfield shift of *p*-carborane carbons and all the aromatic carbons signals of **3** in 15%**3**@TPP-d_{12} means that the whole rotor **3** is inserted inside the TPP-d_{12} channels. While the NMR and X-ray both show a hexagonal inclusion compound, the X-ray clearly shows the presence of both empty hexagonal TPP and monoclinic TPP. The absence of monoclinic TPP signals in the ^{31}P SPE MAS solid-state NMR spectrum demonstrates that at the time when the inclusion 15%**3**@TPP-d_{12} was prepared, monoclinic TPP-d_{12} was absent. However, over time before the X-ray diffraction was measured, some of the free hexagonal TPP-d_{12} collapsed into the more stable monoclinic form. This was subsequently confirmed by a second ^{31}P SPE MAS solid-state NMR experiment.

Independent structural information was obtained from results of X-ray diffraction, which reflect long-range order and are entirely compatible with the information gleaned from solid-state NMR spectra.

The multiple peaks observed in dielectric spectroscopy for 15%**3**@TPP-d_{12} are consistent with a situation where some of the rotators are near the surface, some are internal to the TPP, and some may interact with neighboring rotators from other bulk-included rotor molecules. The lowest rotational barrier in the inclusion compound 15%**3**@TPP-d_{12} is thought to be due to rotators at the channel end, but fully included in the channel, probably in the first TPP layer. The two higher energy barriers would then be due to rotator rotations in the bulk that have different immediate environments. For instance, one of the barriers could correspond to the rotation of a dipolar rotator located next to a void, and another to a rotator located next to the dipolar rotator end of its neighbor.

The frequency factors again have the usual values and the asymmetry factors are small compared to the barrier heights, indicating largely symmetrical rotational potentials.

Surface versus Bulk Inclusion. It is instructive to compare the inclusion compound formation between TPP and the first rotor guest studied, *n*-$C_{16}H_{33}$–$C_2B_{10}H_{10}$–$C_6H_3Cl_2$,[13] and of the rotor **2** that has been examined presently, *n*-C_5H_{11}–C_6H_4–C_6H_4–$C_2B_{10}H_{10}$–$C_6H_3Cl_2$, which differs only in the choice of shaft. In both cases, the shaft enters the TPP channel readily, as desired. The inclusion of the rotor **2** is most likely of the bulk type (Figure 2C), although surface inclusion with the rotator inserted in the top TPP layer cannot be ruled out. The observation that the same *p*-carborane stopper prevents the entry of the rest of the rotor in the former case, forcing the formation of a surface inclusion compound, while in the latter case, it permits the rotator to insert into the channel, is quite remarkable. It suggests the existence of a fine balance between the energy needed to stretch the diameter of the TPP channels, the lattice energy of the guest, and the energy gained from the guest–host interaction. Considerable additional experimentation will be required before the balance is understood in detail and rotors specifically designed for surface inclusion or bulk inclusion can be designed confidently. Apparently, objects whose diameter exceeds the nominal channel width may be

dx.doi.org/10.1021/jo3009897 | J. Org. Chem. XXXX, XXX, XXX–XXX

accommodated quite readily as long as they fit into a single layer.

Initial tentative conclusions are (i) the moieties adjacent to the stopper should not make it easier to stretch the channel diameter, i.e., should not be bulky, and (ii) when the direction of the *p*-carborane symmetry axis is strictly along the channel, the attached rotator does not contribute to the stopping action, whereas when the *p*-carborane axis is tilted, the direction of attachment of the rotator is skewed, permitting it to cooperate as a part of the stopper. The formation of a surface inclusion of type A or B in Figure 2, with a rotator axle normal to the surface, requires the use of a stopper larger than the parent *p*-carborane.

SUMMARY

Inclusion compounds of the rotors **2** and **3** with TPP were prepared and characterized by solid-state NMR, differential scanning calorimetry, X-ray powder diffraction, and dielectric spectroscopy. Annealing was found to be important for their detailed structure. It was critical to use TPP-d_{12} in place of TPP for detailed NMR spectroscopic analysis.

Against expectations, in all inclusion compounds of rotors **2** and **3** were inserted completely into TPP channels, and the *p*-carborane moiety did not act as a stopper.

Longer range structural information from X-ray powder patterns, along with the observed dielectric loss peaks, suggest that in **2**@TPP all rotators, while included into the TPP channel, are near the crystal surface, whereas **3**@TPP is more likely a true fully bulk inclusion compound, with an associated range of local structural variations around the rotator. The rotational barriers observed for both inclusion systems are high compared with expectations for the isolated rotor molecule, indicating the presence of substantial steric hindrance to rotation of the dichlorophenyl rotator included in a TPP channel.

EXPERIMENTAL SECTION

NMR Spectroscopy, Differential Scanning Calorimetry, X-ray Diffraction, and Dielectric Spectroscopy. Measurements were made and evaluated as described elsewhere.[13]

Sample Preparation. The synthesis and storage of TPP, catechol-d_6, TPP-d_{12}, and benzene-d_6@TPP-d_{12} followed published procedures.[13] The amounts used in the preparation of inclusion compounds were as follows. Biphenyl@TPP: biphenyl, 3.1 mg; TPP, 180.0 mg (ground). 5%**2**@TPP: **2**, 10.6 mg; TPP, 180.0 mg (ground). 15%**2**@TPP-d_{12}: **2**, 26.8 mg; TPP-d_{12}, 140.0 mg (ball milling for 90 min was followed by annealing for 1 day, ball milling for 120 min, and annealing for 3 days). 15%**3**@TPP-d_{12}: **3**, 24.3 mg; TPP-d_{12}, 150.0 mg (ball milling for 90 min was followed by annealing for 3 days).

Synthesis. *General Methods.* Air-sensitive reactions were carried out under argon, using standard Schlenk techniques. Tetrahydrofuran was distilled from Na/K under argon and dimethylformamide from calcium hydride into a flask with freshly activated 3 Å molecular sieves under reduced pressure. Degassing was performed by the standard freeze–pump–thaw technique (three times). Pyridine, piperidine, diisopropylamine, acetonitrile, and dichloromethane were distilled from calcium hydride under argon. Triethylamine was distilled from calcium hydride or from sodium/benzophenone under argon. Benzene and toluene were distilled from sodium under argon. NMR solvents were kept over molecular sieves (except for D_2O). Molecular sieves (3 and 4 Å) were freshly activated at 500 °C before use, and they were allowed to cool in a vacuum. Cuprous chloride was purchased in sealed ampules and handled in a glovebox. Only pure white cuprous chloride was used in reactions. All chemicals were used as received.

*4-Nitro-4′-n-pentylbiphenyl (**4**).* A dried high-pressure Schlenk flask (500 mL) with triply sealed Teflon valve was equipped with a magnetic stir bar and a septum. It was charged with *p*-pentylbromobenzene (6.00 g, 26.42 mmol, 1.2 equiv), evacuated, and filled with argon (three times). Anhydrous THF (80 mL) was added, and the solution was cooled in an acetone/dry ice bath. After 5 min, 1.6 M solution of *n*-BuLi in hexanes (16.6 mL, 26.42 mmol, 1.2 equiv) was added to the stirred solution. After 10 min, 1.0 M solution of zinc chloride (52.8 mL, 26.42 mmol, 1.2 equiv) was added, and the resulting mixture was allowed to warm to room temperature. A suspension of *p*-iodonitrobenzene (5.48 g, 22.01 mmol, 1.0 equiv) and tetrakis(triphenylphosphino)palladium (763 mg, 0.66 mmol, 3 mol %) in anhydrous THF (20 mL) was added to the mixture. The valve was then closed, and the reaction mixture was stirred at room temperature for 48 h. The solvent was removed under reduced pressure, and the residue was dissolved in dichloromethane (300 mL). The solution was washed with 10% hydrochloric acid (2 × 100 mL) and water (2 × 100 mL). The organic layer was dried over anhydrous sodium sulfate, filtered, and the solvents were removed under reduced pressure. The crude product was purified by flash chromatography in hexanes and toluene (3/1) to yield 4.969 g (84%) of **4** as yellow crystals: mp (CH_2Cl_2) 46 °C; ^{1}H NMR (400 MHz, $CDCl_3$) δ 8.31–8.25 (m, 2H), 7.76–7.69 (m, 2H), 7.59–7.52 (m, 2H), 7.32 (d, J = 8.3 Hz, 2H), 2.76–2.60 (m, 2H), 1.67 (ddd, J = 15.1, 8.3, 4.8 Hz, 2H), 1.43–1.30 (m, 4H), 0.97–0.87 (m, 3H); ^{13}C{^{1}H} NMR (101 MHz, $CDCl_3$) δ 147.7 (s), 146.9 (s), 144.2 (s), 136.1 (s), 129.3 (s), 127.6 (s), 127.3 (s), 124.2 (s), 35.7 (s), 31.6 (s), 31.2 (s), 22.7 (s), 14.2 (s); IR (KBr, cm^{-1}) 398, 450, 488, 509, 529, 543, 693, 731, 746, 755, 812, 847, 854, 866, 895, 950, 962, 969, 1004, 1023, 1108, 1127, 1176, 1186, 1234, 1250, 1288, 1308, 1339, 1398, 1429, 1454, 1466, 1483, 1513, 1562, 1808, 1917, 1932, 2343, 2858, 2869, 2926, 2954, 2966, 3028, 3077; HRMS (ESI-TOF) 270.1488 (calcd. for MH$^+$: 270.1491); UV–vis (CH_2Cl_2, nm) λ_{max} (ε_{max}) 324 (23700). Elemental analysis calcd. for $C_{17}H_{19}NO_2$ C: 75.81%, H: 7.11%, N: 5.20%. Found C: 75.71%, H: 7.23%, N: 5.25%.

*4-Amino-4′-n-pentylbiphenyl (**5**).* A round-bottom flask (500 mL) was charged with **4** (4.80 g, 17.820 mmol, 1.0 equiv), powdered tin (15.00 g, 126.24 mmol, 7 equiv), concentrated hydrochloric acid (80 mL), water (80 mL) and ethanol (50 mL). The resulting mixture was refluxed for 6 h. The solvents were removed under reduced pressure, the remaining solid was suspended in water (100 mL), and 10% sodium carbonate was added to pH = 9. The solids were filtered, washed with water, and dried. The product was extracted with boiling ethanol, and the suspension was filtered hot. The solvent was removed under reduced pressure to give 4.024 g (94%) of white crystalline **5**: mp (CH_2Cl_2) 69 °C; ^{1}H NMR (400 MHz, $CDCl_3$) δ 7.47–7.43 (m, 2H), 7.43–7.38 (m, 2H), 7.23–7.18 (m, 2H), 6.78–6.72 (m, 2H), 3.70 (s, 2H), 2.68–2.55 (m, 2H), 1.70–1.58 (m, 2H), 1.40–1.28 (m, 4H), 0.96–0.84 (m, 3H); ^{13}C{^{1}H} NMR (101 MHz, $CDCl_3$) δ 145.7 (s), 141.2 (s), 138.6 (s), 131.8 (s), 128.9 (s), 128.0 (s), 126.4 (s), 115.5 (s), 35.7 (s), 31.7 (s), 31.4 (s), 22.7 (s), 14.2 (s); IR (KBr, cm^{-1}) 459, 479, 504, 547, 569, 673, 714, 727, 751, 804, 832, 843, 999, 1134, 1177, 1200, 1230, 1273, 1374, 1403, 1429, 1453, 1466, 1500, 1529, 1579, 1606, 1624, 1886, 1900, 2855, 2868, 2922, 2950, 3026, 3198, 3214, 3304, 3384; UV–vis (CH_2Cl_2, nm) λ_{max} (ε_{max}) 280 (41590). MS (ESI-TOF) 240.2 (calcd. for MH$^+$: 240.2). Elemental analysis calcd. for $C_{17}H_{21}N$ C: 85.30%, H: 8.84%, N: 5.85%. Found C: 85.28%, H: 9.02%, N: 5.89%.

*4-Iodo-4′-n-pentylbiphenyl (**6**).* A round-bottom flask (500 mL) was charged with **5** (3.80 g, 1.0 equiv), water (160 mL) and concentrated sulfuric acid (30 mL), and the suspension was sonicated for 1 h. The resulting fine suspension was cooled to 0 °C, and a solution of sodium nitrite (2.19 g, 31.748 mmol, 2.0 equiv) in water (30 mL) was added dropwise with vigorous stirring. The temperature of the reaction mixture was kept below 5 °C during the addition. After 2 h at 0–5 °C a solution of urea (5 g) in water was added dropwise to the reaction mixture while the temperature was kept below 5 °C. Then, the reaction mixture was slowly poured into a hot (80–90 °C) solution of potassium iodide (15 g) in water (100 mL), and the mixture was stirred for 1 h. The product was extracted into diethyl

dx.doi.org/10.1021/jo3009897 | J. Org. Chem. XXXX, XXX, XXX–XXX

ether (3 × 200 mL), the combined organic layers were washed with 10% sodium thiosulfate (2 × 100 mL), the organic layer was dried over anhydrous sodium sulfate, filtered, and the solvents were removed under reduced pressure. The crude product was purified by flash chromatography in hexanes and toluene (3/1) to yield 4.652 g (84%) of **6** as white crystals: mp (CH_2Cl_2) 110 °C; ^{1}H NMR (400 MHz, $CDCl_3$) δ 7.82−7.74 (m, 2H), 7.54−7.47 (m, 2H), 7.39−7.33 (m, 2H), 7.33−7.27 (m, 2H), 2.78−2.64 (m, 2H), 1.77−1.64 (m, 2H), 1.47−1.33 (m, 4H), 1.03−0.91 (m, 3H); ^{13}C{^{1}H} NMR (101 MHz, $CDCl_3$) δ 142.7 (s), 140.7 (s), 137.9 (s), 137.4 (s), 129.1 (s), 128.6 (s), 126.8 (s), 92.8 (s), 35.7 (s), 31.7 (s), 31.3 (s), 22.7 (s), 14.2 (s); IR (KBr, cm^{-1}) 478, 500, 550, 616, 642, 673, 698, 725, 737, 754, 802, 825, 852, 999, 1066, 1110, 1133, 1276, 1376, 1386, 1456, 1466, 1479, 1519, 1550, 1581, 1607, 1644, 1906, 2852, 2866, 2922, 2949, 3026, 3059; UV−vis (CH_2Cl_2, nm) λ_{max} (ε_{max}) 266 (24210); HRMS (EI-TOF) 350.0529 (calcd. for $C_{17}H_{19}I^+$: 350.0532).

General Procedure for Ulmann Coupling with p-Carboranes. A pressure Schlenk flask (25 to 50 mL), equipped with a triply sealed pressure valve, a magnetic stir bar, a septum and a hose connector, was charged with the *p*-carborane derivative (1 mmol, 1.0 equiv or 5 mmol, 5.0 equiv if *p*-carborane was the starting compound) and with cuprous chloride (1.3 mmol, 1.3 equiv) in a glovebox. The flask was closed, taken outside the glovebox and connected to the Schlenk line. THF (10 mL) was added through the septum under argon, and the resulting mixture was cooled in an acetone/dry ice bath. After 5 min of stirring, *n*-BuLi (1.6 M solution in hexanes, 0.75 mL, 1.2 equiv) was added dropwise under argon. The reaction mixture was stirred for 15 min at −78 °C and then for 30 min at room temperature. Anhydrous pyridine (1 mL) was added to the mixture, and it was stirred until all the cuprous chloride dissolved. The flask was then closed, and a solvent trap was connected to it. The trap was evacuated and filled with argon three times. The trap was then evacuated and cooled with liquid nitrogen. Special precaution was taken to seal all leaks. The reaction mixture was stirred vigorously and slowly opened to the trap. The solvents were removed under reduced pressure, and the flask was filled with argon. After that, a suspension/solution of the iodo derivative (1.5 mmol, 1.5 equiv) in anhydrous DMF (5 to 10 mL) was added under argon. The resulting mixture was heated in a closed vessel at 120 °C for 24 h and then at 140−150 °C for 24−48 h. The reaction progress was monitored by ^{1}H NMR. After the reaction was complete, the solvents were removed under reduced pressure, and the solids were dissolved in dichloromethane (50−150 mL), washed with 5% hydrochloric acid (50 mL), with 10% ammonium hydroxide (2 × 50 mL), and with water (50 mL). The organic layer was dried over anhydrous sodium sulfate, filtered and concentrated under reduced pressure. If *p*-carborane was used in the reaction, it was recovered by sublimation under reduced pressure. The crude product was purified by column chromatography.

*1-(4′-n-Pentylbiphenyl-4-yl)dicarba-closo-dodecaborane (**7**).* The general Ulmann coupling procedure was followed, starting with 800 mg (2.284 mmol) of **6**. The product was purified by column chromatography in hexanes and toluene (3/1) to yield 773.1 mg (92%) of **7** as white crystals: mp (CH_2Cl_2) 79 °C; ^{1}H NMR (300 MHz, $CDCl_3$) δ 7.48−7.34 (m, 4H), 7.31−7.21 (m, 4H), 2.70−2.56 (m, 2H), 3.67−1.86 (m, 10H), 1.74−1.59 (m, 2H), 1.42−1.27 (m, 4H), 1.00−0.86 (m, 3H); ^{13}C{^{1}H} NMR (101 MHz, $CDCl_3$) δ 142.7 (s), 141.3 (s), 137.4 (s), 135.6 (s), 129.0 (s), 127.5 (s), 127.0 (s), 126.6 (s), 86.4 (s), 59.9 (s), 35.7 (s), 31.7 (s), 31.3 (s), 22.7 (s), 14.2 (s); ^{11}B{^{1}H} NMR (96 MHz, $CDCl_3$) δ −12.20 (s), −14.89 (s); IR (KBr, cm^{-1}) 505, 548, 582, 693, 721, 726, 737, 749, 768, 786, 801, 846, 896, 912, 939, 1004, 1016, 1022, 1040, 1090, 1124, 1140, 1147, 1193, 1374, 1397, 1429, 1451, 1464, 1501, 1529, 1577, 1906, 2609, 2856, 2866, 2926, 2951, 3027, 3060; UV−vis (CH_2Cl_2, nm) λ_{max} (ε_{max}) 264 (27030). Elemental analysis calcd for $C_{19}H_{30}B_{10}$ C: 62.26%, H: 8.25%. Found C: 62.02%, H: 8.36%.

*1-(4′-n-Pentylbiphenyl-4-yl)-12-(2,3-dichlorophenyl)-p-dicarba-closo-dodecaborane (**2**).* The general Ulmann coupling procedure was followed, starting with 200.0 mg (0.546 mmol) of **7**. The product was purified by column chromatography in hexane and toluene (3/1) to yield 241.7 mg (87%) of **2** as white crystals: mp (CH_2Cl_2) 152 °C; ^{1}H NMR (500 MHz, CDCl3) δ 7.60 (dd, J = 8.4, 1.4 Hz, 1H), 7.48−7.37 (m, 5H), 7.32−7.28 (m, 2H), 7.25 (t, J = 6.3 Hz, 2H), 7.09−7.04 (m, 1H), 2.67−2.60 (m, 2H), 3.59−2.05 (m, 10H), 1.71−1.59 (m, 2H), 1.42−1.29 (m, 4H), 0.91 (t, J = 7.0 Hz, 3H); ^{13}C{^{1}H} NMR (101 MHz, $CDCl_3$) δ 142.7 (s), 141.6 (s), 137.3 (s), 135.9 (s), 135.0 (s), 134.2 (s), 131.5 (s), 131.0 (s), 130.7 (s), 129.0 (s), 127.5 (s), 127.0 (s), 126.7 (s), 126.7 (s), 86.6 (s), 81.7 (s), 35.7 (s), 31.7 (s), 31.3 (s), 22.7 (s), 14.2 (s); ^{11}B{^{1}H} NMR (96 MHz, CDCl3) δ −12.25 (s); IR (KBr, cm^{-1}) 462, 488, 514, 548, 593, 607, 660, 698, 738, 758, 790, 805, 848, 861, 871, 901, 933, 1004, 1059, 1069, 1082, 1123, 1164, 1194, 1301, 1347,1375, 1398, 1421, 1450, 1464, 1493, 1501, 1561, 1578, 1866, 1904, 1931, 1956, 2613, 2852, 2867, 2927, 2951, 3030, 3051, 3088; HRMS (ESI-TOF) 535.2751 (calcd. for MNa^+: 535.2758); UV−vis (CH_2Cl_2, nm) λ_{max} (ε_{max}) 269 (33950). Elemental analysis calcd. for $C_{25}H_{32}B_{10}Cl_2$: 58.70%, H: 6.31%. Found C: 58.46%, H: 6.41%.

*1,12-Bis(2,3-dichlorophenyl)-p-dicarba-closo-dodecaborane (**3**).* The general Ulmann coupling procedure was followed, starting with 150 mg (1.0 equiv) of *p*-carborane, 1.95 mL (3.0 equiv) of 1.6 M *n*-BuLi, and with 329.0 mg (4.0 equiv) of 1,2-dichloro-3-iodobenzene. The product was purified by column chromatography in pentanes and toluene (2/1), and the product was further purified by crystallization from cyclohexane to yield 345.0 mg (76%) of white crystalline product: mp (CH_2Cl_2) 265 °C; ^{1}H NMR (500 MHz, $CDCl_3$) δ 7.56 (dd, J = 8.4, 1.5 Hz, 2H), 7.41 (dd, J = 7.9, 1.5 Hz, 2H), 7.07 (t, J = 8.1 Hz, 2H), 2.10−3.70 (m, 10H); ^{13}C{^{1}H} NMR (75 MHz, $CDCl_3$) δ−136.0 (s), 134.0 (s), 131.4 (s), 131.2 (s), 130.5 (s), 126.7 (s), 77.4 (s); ^{11}B{^{1}H}NMR (96 MHz, $CDCl_3$) δ −11.89 (s); IR (KBr, cm^{-1}) 484, 685, 699, 738, 747, 762, 796, 814, 867, 947, 964, 1000, 1040, 1057, 1067, 1080, 1124, 1137, 1166, 1207, 1227, 1245, 1304, 1313, 1348, 1378, 1398, 1448, 1557, 1578, 1604, 1643, 1682, 1700, 1715, 1734, 1874, 1943, 2595, 2607, 2636, 2643, 3060, 3100; HRMS (ESI-TOF) 469.0680 (calcd. for MCl^-: 469.0695); UV−vis (CH_2Cl_2, nm) λ_{max} (ε_{max}) 241 (15630), 230 (26490). Elemental analysis calcd. for $C_{14}H_{16}B_{10}Cl_4$ C: 38.73%, H: 3.71%. Found C: 38.88%, H: 3.68%.

■ ASSOCIATED CONTENT

Ⓢ Supporting Information

Results for biphenyl@TPP, Figures S1−S5, NMR assignments for **2**, and NMR spectra for compounds **2**−**7**, Figures S6−12. This material is available free of charge via the Internet at http://pubs.acs.org.

■ AUTHOR INFORMATION

Corresponding Author

*E-mail: michl@eefus.colorado.edu.

Notes

The authors declare no competing financial interest.

■ ACKNOWLEDGMENTS

The research leading to these results has received funding from the European Research Council (FP7/2007-2013/ERC Grant 227756) and from the U.S. National Science Foundation (CHE 0848663 and Materials Research Science and Engineering Centers Grant No. DMR-0820579). We thank Professors Piero Sozzani and Angiolina Comotti (Milan, Italy) for useful discussions.

■ REFERENCES

(1) Kottas, G. S.; Clarke, L. I.; Horinek, D.; Michl, J. *Chem. Rev.* **2005**, *105*, 1281.

(2) Khuong, T.-A. V.; Nunez, J. E.; Godinez, C. E.; Garcia-Garibay, M. A. *Acc. Chem. Res.* **2006**, *39*, 413.

(3) Horansky, R. D.; Magnera, T. F.; Price, J. C.; Michl, J. In *Controlled Nanoscale Motion*; Linke, H., Månsson, A., Eds.; Springer: Berlin, 2007; Lecture Notes in Physics, Vol. *711*, p 303.

(4) Crowly, J. D.; Kay, E. R.; Leigh, D. A. *Intell. Mater.* **2008**, 1.
(5) Garcia-Garibay, M. A. *Nat. Mater.* **2008**, *7*, 431.
(6) Michl, J.; Sykes, E. C. H. *ACS Nano* **2009**, *3*, 1042.
(7) Augulis, R.; Klok, M.; Feringa, B. L. *Phys. Status Solidi C* **2009**, *6*, 181.
(8) Dominiguez, Z.; Dang, H.; Strouse, M. J.; Garcia-Garibay, M. A. *J. Am. Chem. Soc.* **2002**, *124*, 2398.
(9) Rodriguez-Molina, B.; Ochoa, M. E.; Farfan, N.; Santillan, R.; Garcia-Garibay, M. A. *J. Org. Lett.* **2009**, *74*, 8554.
(10) Karlen, S. D.; Reyes, H.; Taylor, R. E.; Khan, S. I.; Hawthorne, M. F.; Garcia-Garibay, M. A. *Proc. Natl. Acad. Sci. U. S. A.* **2010**, *107*, 14973.
(11) Lemouchi, C.; Vogelsberg, C. S.; Zorina, L.; Simonov, S.; Batail, P.; Brown, S.; Garcia-Garibay, M. A. *J. Am. Chem. Soc.* **2011**, *133*, 6371.
(12) Horansky, R. D.; Clarke, L. I.; Winston, E. B.; Price, J. C.; Karlen, S. D.; Jarowski, P. D.; Santillan, R.; Garcia-Garibay, M. A. *Phys. Rev. B* **2006**, *74*, 054306.
(13) Kobr, L.; Zhao, K.; Shen, Y.; Comotti, A.; Bracco, S.; Shoemaker, R. K.; Sozzani, P.; Clark, N. A.; Price, J. C.; Rogers, C. T.; Michl, J. *J. Am. Chem. Soc.* **2012**, *134*, 10122.
(14) Winston, E. B.; Lowell, P. J.; Vacek, J.; Chocholoušová, J.; Michl, J.; Price, J. C. *Phys. Chem. Chem. Phys.* **2008**, *10*, 5188.
(15) Gould, S. L.; Tranchemontagne, D.; Yaghi, O. M.; Garcia-Garibay, M. A. *J. Am. Chem. Soc.* **2008**, *130*, 3246.
(16) Allcock, H. R.; Siegel, L. A. *J. Am. Chem. Soc.* **1964**, *86*, 5140.
(17) Comotti, A.; Simonutti, R.; Stramare, S.; Sozzani, P. *Nanotechnology* **1999**, *10*, 70.
(18) Sozzani, P.; Bracco, S.; Comotti, A.; Ferretti, L.; Simonuti, R. *Angew. Chem., Int. Ed.* **2005**, *44*, 1816.
(19) Brustolon, M.; Barbon, A.; Bortolus, M.; Maniero, A. L.; Sozzani, P.; Comotti, A.; Simonutti, R. *J. Am. Chem. Soc.* **2004**, *126*, 15512.
(20) Sozzani, P.; Comotti, A.; Bracco, S.; Simonutti, R. *Angew. Chem., Int. Ed.* **2004**, *43*, 2792.
(21) Allcock, H. R.; Levin, M. L.; Whittle, R. R. *Inorg. Chem.* **1986**, *25*, 41.
(22) Primrose, A. P.; Parvez, M.; Allcock, H. R. *Macromolecules* **1997**, *30*, 670.
(23) Allcock, H. R. *J. Am. Chem. Soc.* **1963**, *85*, 4050.
(24) Allcock, H. R. *J. Am. Chem. Soc.* **1964**, *86*, 2591.
(25) Allcock, H. R.; Allen, R. W.; Bissell, E. C; Smeltz, L. A.; Teeter, M. *J. Am. Chem. Soc.* **1976**, *98*, 5120.
(26) Kobr, L.; Zhao, K.; Shen, Y.; Shoemaker, R. K.; Rogers, C. T.; Michl, J. submitted for publication.
(27) Schöberl, U.; Magnera, T. F.; Harrison, R.; Fleischer, F.; Pflug, J. L.; Schwab, P. F. H.; Meng, X.; Lipiak, D.; Noll, B. C.; Allured, V. S.; Rudalevige, T.; Lee, S.; Michl, J. *J. Am. Chem. Soc.* **1997**, *119*, 3907.
(28) Comotti, A.; Bracco, S.; Ferretti, L.; Mauri, M.; Simonutti, R.; Sozzani, P. *Chem. Commun.* **2007**, 350.
(29) Bohn, R. K.; Bohn, M. D. *Inorg. Chem.* **1971**, *10*, 350.
(30) Hurdis, E. C.; Smyth, C. P. *J. Am. Chem. Soc.* **1942**, *64*, 2212.
(31) Masao, O.; Mariko, U.; Masahiko, A.; Junko, Y.; Ichiro, Y. *J. Mol. Struct.* **1986**, *147*, 77.
(32) Sozzani, P.; Comotti, A.; Simonutti, R.; Meersmann, T.; Logan, J. W.; Pines, A. *Angew. Chem. Int Ed.* **2000**, *39*, 2695.
(33) Silverstein, R. M.; Webster, F. X. *Spectrometric Identification of Organic Compounds*, 6th ed.; John Wilez and Sons: New York, 1998.
(34) Tonelli, A. *NMR Spectroscopy and Polymer Microstructure: The Conformational Connection*; VCH Publishers: Deerfeld Beach, FL, 1988.
(35) Comotti, A.; Simonutti, R.; Catel, G; Sozzani, P. *Chem. Mater.* **1999**, *11*, 1476.
(36) Sozzani, P.; Bovey, F. A.; Schilling, F. C. *Macromolecules* **1991**, *24*, 6764.